

Interference of scattering pathways in Raman heterodyne spectroscopy of multilevel atoms

Tilo Blasberg and Dieter Suter

Institut für Quantenelektronik, Eidgenössische Technische Hochschule Zürich, CH-8093 Zürich, Switzerland

(Received 5 December 1994)

Raman heterodyne detection of nuclear magnetic resonance is a sensitive technique for optical detection of an NMR transition, which is driven by a resonant radio-frequency field. The observed signal is linear in the transition matrix elements of the magnetic resonance transition and two optical transitions. This linearity is the reason that signal contributions from different sites or different rf transitions can interfere, in many cases destructively. In this article, we discuss such an interference effect, which appears to have been overlooked in the past. It occurs between signal contributions that originate from the same magnetic resonance transition of atoms with different positions within the inhomogeneously broadened optical resonance line. These atoms contribute to the coherent Raman scattering through different scattering paths, which involve optical transitions to different nuclear spin states of the same electronic state. We show that the interference between all possible scattering paths leads to complete signal cancellation, if the atoms that are involved in the different scattering paths are equally polarized. To study the effect and to eliminate the interference, we used a pump-and-probe technique with two laser beams. With two independent laser frequencies, it becomes possible to separate the individual scattering paths. We calculate the dependence of the signal on the frequency of both laser beams as well as on the radio frequency and compare the results to experimental data from $\text{Pr}^{3+}:\text{YAlO}_3$. Our results show that the interference reduces the signal amplitude of the conventional Raman heterodyne experiment but can be eliminated in the new experiment.

INTRODUCTION

Raman heterodyne detection of nuclear magnetic resonance (NMR) (Ref. 1) uses laser radiation to detect nuclear spin transitions whose frequencies are in the MHz range. Compared to conventional magnetic resonance, it provides a much higher sensitivity and allows to correlate optical and nuclear spin effects.² The technique relies on coherent Raman scattering, thus making the observed frequency resolution independent of the laser linewidth. After its initial observation,^{1,3} it was applied to various rare-earth ionic solids, e.g., $\text{Pr}^{3+}:\text{LaF}_3$,^{1,4,5} $\text{Pr}^{3+}:\text{YAlO}_3$,⁶⁻⁸ or $\text{Eu}^{3+}:\text{YAlO}_3$.⁹ Recently the technique could be extended on the detection of electron paramagnetic resonance (EPR) in diamond.¹⁰

In the Raman heterodyne experiment, a resonant rf field and a laser field drive an atomic system and excite a coherent superposition between two nuclear spin states. The same laser beam that is involved in the excitation of this coherence undergoes coherent Raman scattering.^{11,12} The Raman field propagates collinearly with the incident laser field. On a quadratic detector, the two fields give rise to a beat signal that is proportional to the sublevel coherence. In the simplest case, the Raman heterodyne experiment involves three energy levels. One of the three transitions contains the coherent excitation of the medium, while the two other transitions couple to the incident laser field and the scattered Raman field. The signal is linear in the matrix elements of all three transitions.

The systems on which Raman heterodyne experiments are performed, contain many three-level systems that allow Raman scattering processes. Since the signal is linear

in the matrix elements, contributions from different scattering processes can interfere. Destructive interference of different scattering paths associated with different Zeeman sublevels or nonequivalent lattice sites in $\text{Pr}^{3+}:\text{YAlO}_3$ (YAP) was investigated by various groups.^{6,7,13,14} It is known, that each of the two interference effects can prevent the observation of a Raman heterodyne signal in zero magnetic field.

In this article, we investigate an additional interference mechanism that occurs even for a single magnetic resonance transition. It is associated with the interference of more than two (in our system six) scattering paths. These multiple scattering paths become possible, whenever the true energy level structure of the atomic system contains more than three energy levels. Since the inhomogeneous line broadening in rare-earth ionic solids exceeds the energetic separations between nuclear spin states by several orders of magnitude, a laser field can simultaneously be in resonance with all possible optical transitions for different ensembles of multilevel atoms. As a consequence, all possible scattering paths contribute to the signal. Since these scattering paths include all states of a complete set of eigenfunctions a complete destructive interference is possible.

In the conventional Raman heterodyne experiment, the individual signal contributions cannot be separated. The sum over all transition matrix elements adds to zero, but complete signal cancellation is avoided when the population differences associated with the various pathways are not identical. We present here an experimental scheme that uses two independent laser beams to avoid these destructive interference effects and investigate the individual

scattering paths separately. In our triple-resonance experiment only those atoms can contribute to the signal, which simultaneously interact with the resonant rf field and two independent laser fields.

This article is structured as follows. After a brief introduction into the energy level structure of the model system $\text{Pr}^{3+}:\text{YAP}$, we introduce the principle of Raman heterodyne experiments with two laser beams. We derive first an expression for the signal amplitude and discuss then its dependence on the detuning of the radio-frequency and laser fields. We then compare the calculated line shapes to experimental data, discuss the relations between resonance lines associated with different scattering paths, and demonstrate the occurrence of the predicted interference effects. The paper concludes with a summary of the main results and a discussion of the consequences for Raman heterodyne experiments in general.

ENERGY LEVEL STRUCTURE

The experiments that we discuss here were performed on the rare-earth ionic solid $\text{Pr}^{3+}:\text{YAIO}_3$ (YAP). In this solid the combined effect of pure nuclear quadrupole,^{15,16} and pseudoquadrupole interaction¹⁷ lifts the degeneracy of the nuclear spin sublevels in the electronic ground state and in the electronically excited state. The spin Hamiltonian of the pseudoquadrupole interaction can be written as

$$\mathcal{H}_Q = D \left[I_z^2 - \frac{1}{3}I(I+1) + \frac{\eta}{3}[I_x^2 - I_y^2] \right], \quad (1)$$

where the coupling constant D depends on the nuclear quadrupole moment and the electric-field gradient tensor at the site of the nucleus¹⁵ as well as on the hyperfine coupling and the crystal field.¹⁷ The asymmetry parameter η , which parametrizes the deviation from an axially symmetric tensor, falls in the range $0 \leq \eta \leq 1$.

For Pr^{3+} ions with a nuclear spin $I = \frac{5}{2}$, the eigenvalue spectrum consists of three pairs of doubly degenerate states with $m_I = \pm\frac{1}{2}$, $\pm\frac{3}{2}$, and $\pm\frac{5}{2}$. Depending on the sign of the quadrupole coupling constant D , either the states with $m_I = \pm\frac{5}{2}$ ($D < 0$) or with $m_I = \pm\frac{1}{2}$ ($D > 0$) are the energetically lowest states. Using the new spectroscopic technique, which we describe below, we could show that in the electronic ground state of $\text{Pr}:\text{YAP}$ the coupling constant is negative, $D_g < 0$.¹⁸ The literature contains no information about the sign of the coupling constant in the excited state, but our experimental data favor a negative coupling constant, $D_e < 0$. $\text{Pr}:\text{YAP}$ is an ideal model system for the demonstration of two-beam Raman heterodyne experiments, as the sublevel splittings in the electronic ground state (7, 14, and 21 MHz) are considerably larger than in the excited state (0.9, 1.6, and 2.5 MHz).

PRINCIPLE OF TWO-BEAM RAMAN HETERODYNE SPECTROSCOPY

To introduce the two-beam Raman heterodyne experiment, we use the simplified level scheme of Fig. 1. The states $|0\rangle$, $|1\rangle$, and $|2\rangle$ represent nuclear spin states in

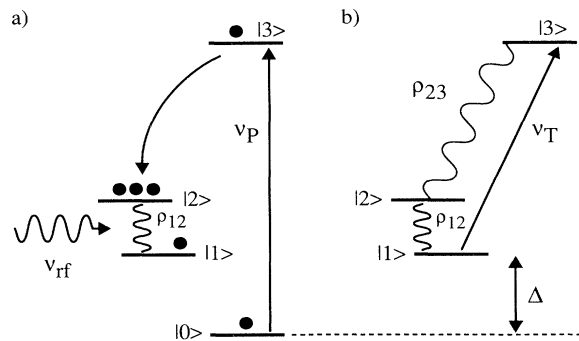


FIG. 1. Principle of Raman heterodyne detection of NMR with two laser beams. (a) The pump laser field, which couples to transition $|0\rangle \leftrightarrow |3\rangle$, creates a population difference for transition $|1\rangle \leftrightarrow |2\rangle$. A resonant rf field converts this population difference into coherence. (b) The test laser field is resonant with the transition $|1\rangle \leftrightarrow |3\rangle$ of the same atoms. Coherent Raman scattering creates a Raman field in transition $|2\rangle \leftrightarrow |3\rangle$.

electronic ground state and $|3\rangle$ represents the electronically excited state, where we neglect, for the time being, the existence of nondegenerate sublevels. The pump laser field with frequency ν_P , which couples to the optical transition between ground-state sublevel $|0\rangle$ and the excited state, depletes the population of ground-state sublevel $|0\rangle$ by spectral hole burning. If the excited state can decay to other ground-state sublevels, the pump laser field establishes a population difference between the ground-state sublevels $|2\rangle$ and $|1\rangle$. The radio-frequency field with frequency ν_{rf} , which drives the nuclear spin transition between sublevels $|1\rangle$ and $|2\rangle$, converts this population difference into coherence between these two states.

The right-hand part of Fig. 1 illustrates the Raman heterodyne detection of the sublevel coherence. If the test laser field with frequency ν_T couples to the optical transition $|1\rangle \leftrightarrow |3\rangle$, the sublevel coherence induces coherent Raman scattering,¹² exciting a Raman field in the adjacent optical transition, in this case in transition $|2\rangle \leftrightarrow |3\rangle$. Behind the sample, the scattered Raman field and the test laser field interfere and the frequency difference between the two fields becomes observable as a beat signal.

This simple description has to be modified if the experiment is performed on systems where the inhomogeneous line broadening is much larger than the sublevel splittings between the nuclear spin states. As a consequence of the inhomogeneous line broadening, a laser field can couple to each of the optical transitions for different subsets of atoms. For a model atom with two nondegenerate sublevels in the ground state $|g\rangle$ and in the electronically excited state $|e\rangle$, the left-hand part of Fig. 2 shows all four optical transitions to which a pump laser field of frequency ν_P can couple. Each optical transition represents a different subset of atoms that contributes to the inhomogeneously broadened absorption line.

In a pump-and-probe experiment performed on multilevel atoms, one can only observe a signal, if the pump and probe laser interact with the same set of atoms. The

cess with a relaxation rate γ_B . The equation of motion in the rotating frame is then

$$\dot{\rho}_{21}^{\text{rf}} = -\frac{i}{\hbar} \left[(\delta_{\text{rf}} - i\gamma_B) \bar{\rho}_{21} + \frac{\Omega_{21}}{2} (\rho_{22} - \rho_{11}) \right]. \quad (6)$$

The stationary solution for the sublevel coherence is

$$\rho_{21}^{\text{rf}}(t \rightarrow \infty) = -\frac{(\rho_{22} - \rho_{11})\Omega_{21}}{2(\delta_{\text{rf}} - i\gamma_B)}. \quad (7)$$

The resulting sublevel coherence is linear in the rf-field strength and in the population difference $(\rho_{22} - \rho_{11})$ between the nuclear spin states. Its time evolution in the lab frame is determined by the frequency of the rf field, which drives the sublevel transition, as can be seen by reversing the transformation U_{rf} into the rotating frame.

B. Coherent Raman scattering

Next we discuss the coherent Raman scattering of a resonant test laser field from this sublevel coherence. As indicated in Fig. 3, we assume that the test laser field with frequency $\omega_L + \Delta/2$ couples to the optical transition $|1\rangle \leftrightarrow |3\rangle$ and write the interaction as

$$V_{13} = \langle 1|V(t)|3\rangle = \hbar\Omega_{13} \cos[(\omega_L + \Delta/2)t] = V_{31}^* \quad (8)$$

with the coupling strength $\Omega_{13} = \mu_{13}E_0/\hbar$. The detuning of the test laser field is $\delta_L = \omega_0 - \omega_L$. With a similar transformation as in (4) but with ω_0 replaced by ω_L and with ω_{rf} replaced by Δ

$$U_L = U(\omega_L, \Delta; t)$$

$$= \exp \left[-\frac{it}{6} \begin{pmatrix} 2\omega_L + 3\Delta & 0 & 0 \\ 0 & 2\omega_L - 3\Delta & 0 \\ 0 & 0 & -4\omega_L \end{pmatrix} \right], \quad (9)$$

one can transform the total Hamiltonian $\mathcal{H}_0 + V(t)$ into a second rotating frame

$$\begin{aligned} \mathcal{H}^L &= U_L \mathcal{H} U_L^{-1} + i\dot{U}_L U_L^{-1} \\ &= \hbar \begin{pmatrix} -\frac{\delta_L}{3} & 0 & \frac{\Omega_{13}}{2} \\ 0 & -\frac{\delta_L}{3} & 0 \\ \frac{\Omega_{31}}{2} & 0 & \frac{2\delta_L}{3} \end{pmatrix}. \end{aligned} \quad (10)$$

We denote this rotating frame by a tilde. If the rf field is off resonant, the sublevel coherence $\rho_{12}^{\text{rf}}(t \rightarrow \infty)$ becomes time dependent in this new rotating frame

$$\begin{aligned} \rho^L &= U_L U_{\text{rf}}^{-1} \rho^{\text{rf}} U_{\text{rf}} U_L^{-1}, \\ \rho_{21}^L &= \rho_{21}^{\text{rf}}(t \rightarrow \infty) \exp[i\delta_{\text{rf}} t] \\ &= -\frac{(\rho_{22} - \rho_{11})\Omega_{21}}{2(\delta_{\text{rf}} - i\gamma_B)} \exp[i\delta_{\text{rf}} t] \end{aligned} \quad (11)$$

as can be seen by inspection of the transformations U_{rf}

and U_L .

Coherent Raman scattering corresponds to the excitation of optical coherences by the test laser field. To find the Raman field, we solve the equation of motion for the optical coherences in transition $|2\rangle \leftrightarrow |3\rangle$:

$$\dot{\rho}_{23}^L = \frac{i}{\hbar} \left[(\delta_L + i\gamma_E) \rho_{23}^L + \frac{\Omega_{13}}{2} \rho_{21}^L \right]. \quad (12)$$

Introducing an optical dephasing rate γ_E into the equation of motion we find the stationary solution for the optical coherence in the adjacent optical transition $|2\rangle \leftrightarrow |3\rangle$

$$\rho_{23}^L(t \rightarrow \infty) = -\rho_{21}^{\text{rf}}(t \rightarrow \infty) \frac{\Omega_{13}}{2(\delta_L + i\gamma_E)} \exp[i\delta_{\text{rf}} t]. \quad (13)$$

From Eqs. (13) and (7) one can calculate the polarization of the medium by multiplying the optical coherence with the transition matrix element of the Raman transition and with the density of atoms N . The slowly varying part of the polarization is

$$\begin{aligned} \tilde{P}_{\text{St}} &= 2N\rho_{23}^L(t \rightarrow \infty) \mu_{32} e^{-i\delta_{\text{rf}} t} \\ &= \frac{2N(\rho_{22} - \rho_{11})E_0 B_{\text{rf}} \mu_{13} \mu_{32} \mu_{21}}{(2\hbar)^2 (\delta_L + i\gamma_E) (\delta_{\text{rf}} - i\gamma_B)}, \end{aligned} \quad (14)$$

representing the Fourier amplitude at the Stokes-frequency. The time-dependent polarization is therefore

$$P_{\text{St}}(t) = \frac{1}{2} \tilde{P}_{\text{St}} \exp \left[i \left[\omega_L + \frac{\Delta}{2} - \omega_{\text{rf}} \right] t \right] + \text{c.c.} \quad (15)$$

Macroscopically the polarization corresponds to electric dipoles, which oscillate at a frequency that is lower than that of the incident test laser field. The scattered Raman field is Stokes shifted with respect to the incident test laser field. We label therefore the optical polarization in Eq. (15) with the lower index St. In Fig. 3, the corresponding anti-Stokes process occurs when the laser couples to transition $|2\rangle \leftrightarrow |3\rangle$, creating the Raman field in transition $|1\rangle \leftrightarrow |3\rangle$. The two cases differ only with respect to the indices of the states to which the optical fields couple. We may thus calculate the optical polarization for the anti-Stokes process from that of the Stokes process by interchanging the indices 1 and 2 in the three transition matrix elements and by changing the sign of the population difference $(\rho_{22} - \rho_{11})$ and of the rf detuning δ_{rf} . With these substitutions, we find for the slowly varying amplitude of the optical polarization

$$\begin{aligned} \tilde{P}_{\text{aSt}} &= 2N\rho_{13}^L(t \rightarrow \infty) \mu_{31} e^{i\delta_{\text{rf}} t} \\ &= \frac{2N(\rho_{22} - \rho_{11})E_0 B_{\text{rf}} \mu_{12} \mu_{23} \mu_{31}}{(2\hbar)^2 (\delta_L + i\gamma_E) (\delta_{\text{rf}} + i\gamma_B)}, \end{aligned} \quad (16)$$

which is the Fourier amplitude at the anti-Stokes frequency. The time-dependent polarization is

$$P_{\text{aSt}}(t) = \frac{1}{2} \tilde{P}_{\text{aSt}} \exp \left[i \left[\omega_L - \frac{\Delta}{2} + \omega_{\text{rf}} \right] t \right] + \text{c.c.} \quad (17)$$

Since the same optical transition matrix elements contrib-

ute to the optical polarization, Stokes and anti-Stokes components have the same intensity in the scattered light.¹¹

The polarization of the medium P acts as a source term for the Raman wave, whose buildup is governed by the one-dimensional wave equation

$$\frac{\partial \mathcal{E}_R(z)}{\partial z} = i \frac{\omega_R^2 \mu_0}{2k} \tilde{P} \quad (18)$$

with

$$\omega_R = (\omega_T \mp \omega_{\text{rf}}) \quad \text{and} \quad \omega_T = \left[\omega_L \pm \frac{\Delta}{2} \right]. \quad (19)$$

\mathcal{E}_R and \tilde{P} describe the slowly varying part of the field amplitude and of the polarization, ω_R and ω_T represent the frequencies of the Raman and test laser field; the upper sign refers to Stokes scattering and the lower sign to anti-Stokes scattering of the test laser field. k is the wave vector, μ_0 the magnetic permeability, and z the coordinate in the direction of propagation. The Raman field behind a sample of length L is

$$\mathcal{E}_R(L) = i \frac{\omega_R^2 \mu_0}{2k} L \tilde{P}. \quad (20)$$

The amplitude and phase of the Raman field are thus directly proportional to the optical polarization of the medium.

The total field behind the sample is the superposition of the incident test laser field and the scattered Raman field. We are interested only in the component parallel to the polarization of the incident test laser field, which we write as

$$E_T(t) = \frac{1}{2} (\mathcal{E}_0 e^{i\omega_T t} + \mathcal{E}_R e^{i\omega_R t}) + \text{c.c.} \quad (21)$$

The corresponding intensity is

$$I(t) = \varepsilon_0 c \langle E_T^2(t) \rangle \\ = \frac{1}{2} \omega_R \mathcal{E}_0 L [-\tilde{P}_{\text{Im}} \cos(\omega_{\text{rf}} t) \pm \tilde{P}_{\text{Re}} \sin(\omega_{\text{rf}} t)], \quad (22)$$

where the angle brackets denote the time average over one optical cycle and we have only considered the time-dependent part of the total intensity. For convenience we have separated the real part \tilde{P}_{Re} and the imaginary part \tilde{P}_{Im} of the optical polarization \tilde{P} . The heterodyne beat signal contains an in-phase part [$\propto \cos(\omega_{\text{rf}} t)$] and an out-of-phase part [$\propto \sin(\omega_{\text{rf}} t)$], which can be separated in an experiment using a phase-sensitive detection scheme.

C. Frequency dependence

Using expressions (14) and (16) for the optical polarization, we write the heterodyne signal as

$$S(t) = \frac{A_S}{(\delta_L^2 + \gamma_E^2)(\delta_{\text{rf}}^2 + \gamma_B^2)} [(\pm \delta_L \delta_{\text{rf}} + \gamma_E \gamma_B) \cos(\omega_{\text{rf}} t) \\ + (\pm \delta_L \gamma_B - \delta_{\text{rf}} \gamma_E) \sin(\omega_{\text{rf}} t)], \quad (23)$$

where the amplitude is

$$A_S = \frac{\omega_R \tilde{N}}{(2\hbar)^2} E_0^2 B_{\text{rf}} (\rho_{22} - \rho_{11}) \text{Im} \{ \mu_{12} \mu_{23} \mu_{31} \} \quad (24)$$

and we have used the fact that the triple-product of the transition matrix elements is purely imaginary in all experiments that we discuss here. \tilde{N} represents the number of atoms in the volume that is defined by the length L of the sample and the laser beam area in the sample. The upper sign refers to the Stokes process, the lower to the anti-Stokes process. The signal is directly proportional to the test laser intensity, to the rf-field strength, to the sub-level population difference, and to the triple product of the transition matrix elements. The expression (23) is strictly valid only for a homogeneously broadened system. However, as we will see, the essential features of the signal remain when inhomogeneous line broadening is taken into account.

From Eq. (23), we can recover the case of the conventional Raman heterodyne experiment by setting $\delta_L \rightarrow 0$:

$$S(t; \delta_L = 0) = \frac{A_S}{\gamma_E (\delta_{\text{rf}}^2 + \gamma_B^2)} [\gamma_B \cos(\omega_{\text{rf}} t) - \delta_{\text{rf}} \sin(\omega_{\text{rf}} t)]. \quad (25)$$

This corresponds to the situation of the conventional (single-beam) Raman heterodyne experiment discussed by Wong *et al.*¹ There are two differences between this expression and their Eq. (2.33): they assumed a real triple product of the matrix elements, while it is imaginary in our case. In our case, the in-phase (cos) component of the signal $S(\delta_L = 0)$ has an absorptive dependence on the rf detuning and the out-of-phase (sin) component has a dispersive frequency dependence. The second difference concerns the line shape: while Wong *et al.* performed an average over the inhomogeneously broadened line, resulting in a Gaussian line shape, we consider only an isolated spin with a Lorentzian frequency dependence.

Another limiting case of interest is that of on-resonance irradiation of the magnetic-dipole transition ($\delta_{\text{rf}} = 0$):

$$S(t; \delta_{\text{rf}} = 0) = \frac{A_S}{(\delta_L^2 + \gamma_E^2) \gamma_B} [\gamma_E \cos(\omega_{\text{rf}} t) \pm \delta_L \sin(\omega_{\text{rf}} t)]. \quad (26)$$

Like for the dependence on the radio frequency, the in-phase part of the signal has an absorptive dependence and the out-of-phase part has a dispersive dependence on the detuning of the test laser field. In contrast to the radio-frequency dependence, we expect that in this case the out-of-phase part has an opposite sign for Stokes and anti-Stokes scattering, while the in-phase component remains invariant.

TRIPLE RESONANCE SIGNAL

A. Dependence on laser frequency difference

So far, we have considered only hypothetical three- and four-level systems. The actual system that we con-

sider has six nuclear spin sublevels in the excited and ground state. For a discussion of the signal contributions, we neglect for the moment the existence of sublevels in the excited state. We assume that the pump laser beam drives the system with a fixed frequency and the rf field excites a coherent superposition of the ground-state sublevels $m_I = \pm\frac{1}{2}$ and $\pm\frac{3}{2}$, which are doubly degenerate in the absence of an external magnetic field. Coherent Raman scattering occurs whenever the test laser beam is resonant with the optical transition from one of these two sublevels to the excited state. In the experiment that we consider, the pump laser frequency remains fixed, while the test laser frequency is scanned over a range of ± 25 MHz with respect to the pump laser frequency. The stick spectrum at the top of Fig. 4 indicates for what test laser frequencies one can expect a Raman heterodyne signal (RHS).

A RHS becomes possible when the pump laser beam is resonant with one of the three transitions from one of the ground-state sublevels to the excited state while the test laser is resonant with a transition from the ground-state sublevels $|\pm\frac{1}{2}\rangle$ or $|\pm\frac{3}{2}\rangle$ of the same atom to the excited state. The six possible cases are indicated by the letters in the lower half of Fig. 4, where the letters P and T indicate the ground-state sublevels to which the pump (P) and test (T) laser field couple for a given laser frequency difference. In two cases, the two frequencies coincide, while the four other resonance lines in the spectrum occur at clearly distinct laser frequency differences. As an example, the diagram on the left-hand side of Fig. 4 shows the optical transitions to which pump and test laser field couple for a signal contribution at $\nu_T - \nu_P = -21$ MHz. With two independent laser beams it becomes possible to investigate separately signal contributions of different subsets of atoms. In the following, we refer to this spectrum as the ground-state spectrum, as its frequency differences correspond to the energy level splittings in the electronic ground state.

The spectrum of the RHS becomes more complicated

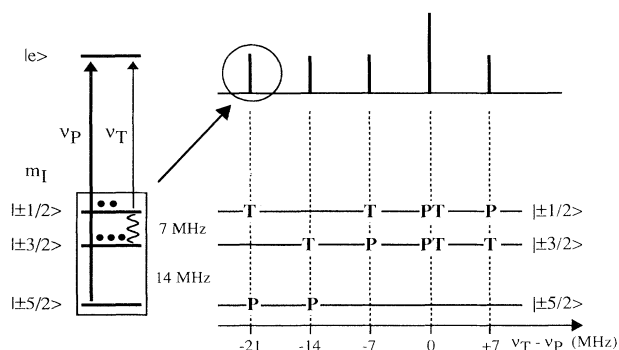


FIG. 4. Theoretical stick spectrum of the two-beam Raman heterodyne signal for the case that a coherent superposition between the nuclear spin substates with $m_I = \pm\frac{1}{2}$ and $\pm\frac{3}{2}$ has been excited in the electronic ground state. For each resonance line the letters indicate the nuclear spin substates which are in resonance with the pump (P) and test (T) laser field. From the overall shape of the spectrum one can derive the energetic order of the nuclear spin states.

if one takes also the nondegenerate sublevels in the electronically excited state into account. Additional resonance lines appear in the spectrum, whenever pump and test laser field couple to a different sublevel of the electronically excited state. Since the sublevel splittings in the excited state of Pr:YAP are approximately one order of magnitude smaller than in the ground state, these resonance lines appear near each of the ground-state resonance lines and can be clearly distinguished from the ground-state spectrum. In the following we will refer to these additional resonance lines as satellite lines. Figure 5 summarizes the different optical configurations that contribute to the spectrum of the satellite lines near the dashed resonance line at $\nu_T - \nu_P = -21$ MHz. For this satellite spectrum the pump laser field couples to ground-state sublevel $|\pm\frac{5}{2}\rangle$ and the test laser field to the sublevel $|\pm\frac{1}{2}\rangle$.

The lower part of Fig. 5 shows the energy level scheme of the excited state (for $D_e < 0$) and explains to which excited state sublevels pump (P) and test (T) laser fields couple at the given position in the spectrum. With three optical transitions to which pump and test laser field can couple, nine different optical configurations contribute to the satellite spectrum. Three of the resonance lines coincide at the position of the ground-state resonance line (dashed line), in the center of the satellite spectrum. At this position pump and test laser field couple to the same excited-state sublevels. For the remaining six satellite lines, pump and test laser fields couple to different sublevels in the excited state. Since optical transitions to each excited state sublevel can contribute to the RHS, the satellite spectrum is symmetric and three satellite lines appear symmetrically on each side of the central line. The positions in the satellite spectrum directly correspond to sublevel splittings in the electronically excited state.

B. Interference of scattering paths

The expression (23) for the heterodyne signal is linear in the product of all three transition matrix elements that are involved in the Raman scattering process. If the total Raman signal consists of more than one signal contribu-

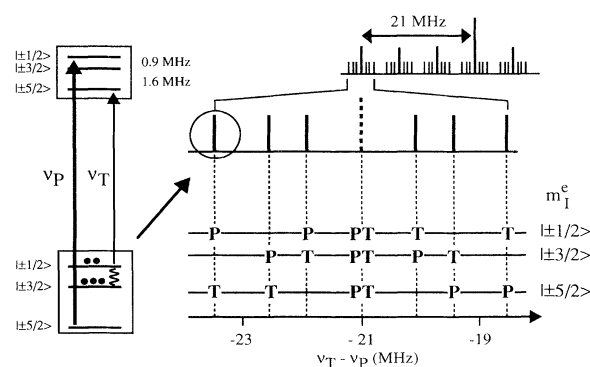


FIG. 5. Theoretical stick spectrum of one satellite spectrum, which arises due to the existence of nondegenerate sublevels in the electronically excited state. For each resonance line the letters indicate the spin substates of the electronically excited state to which the pump (P) and test (T) laser field couple.

tion, interference may lead to distortion and cancellation of the signal. Two destructive interference effects are known for Pr:YAP and related systems:^{6,7,13,14} Site interference, which occurs between signal contributions of nonequivalent lattice sites related by a symmetry operation, and Zeeman interference, which occurs when at least two rf transitions have similar resonance frequencies. Both types of destructive interference can be circumvented by applying an external magnetic field of appropriate strength and orientation: In the magnetic field, the transitions involved in the interference process are nonequivalent and do not interfere any more.

Both interference effects could be explained analytically by Mitsunaga, Kintzer, and Brewer⁷ with the assumption that the quantum-mechanical wave functions of the eigenstates can be factorized into an electronic and a nuclear wave function. With this assumption one can write the wave function of a nuclear spin sublevel in the electronic ground state as $|g\rangle = |\Psi_g\rangle|\chi_g\rangle$ and in the electronically excited state as $|e\rangle = |\Psi_e\rangle|\chi_e\rangle$, where Ψ refers to the electronic degrees of freedom and χ to the nuclear spin variables. The separation makes it possible to factorize the transition matrix element μ_{ge} for an optical transition as

$$\begin{aligned}\mu_{ge} &= \langle g|\boldsymbol{\mu}\cdot\mathbf{E}|e\rangle = \langle \Psi_g|\boldsymbol{\mu}\cdot\mathbf{E}|\Psi_e\rangle\langle \chi_g|\chi_e\rangle \\ &= \mu_{\text{opt}}\langle \chi_g|\chi_e\rangle.\end{aligned}\quad (27)$$

The electric dipole operator acts only on the electronic part of the total wave function and is therefore equal for all optical transitions between the nuclear spin sublevels in the ground and in the excited state. Different matrix elements arise from the overlap integral $\langle \chi_g|\chi_e\rangle$ of the two nuclear spin functions.

As Fig. 5 shows, three different groups of atoms contribute to the central line of the satellite spectrum if the inhomogeneous line broadening exceeds the splitting between nuclear spin sublevels. For all groups, pump laser and radio-frequency field have established a coherent superposition between two ground-state sublevels, e.g., $|\pm\frac{1}{2}\rangle$ and $|\pm\frac{3}{2}\rangle$. The difference between the three contributions is the excited state sublevel to which the pump and test laser field couple. In terms of the detection process, the difference is the "scattering path," i.e., the optical transitions that are involved in the coherent Raman scattering process.

The amplitude of the RHS for each configuration is determined by the triple product of the relevant transition matrix elements and by the population difference between the ground-state sublevels $|\pm\frac{1}{2}\rangle$ and $|\pm\frac{3}{2}\rangle$. To calculate the signal amplitude S of the RHS, we have to add the individual contributions. In the presence of an external magnetic field we have to take into account six signal contributions:

$$\begin{aligned}S &\propto \sum_{e=1}^6 (\rho_{22} - \rho_{11})\mu_{12}\mu_{2e}\mu_{e1} \\ &\cong \Delta\rho\mu_{12}|\mu_{\text{opt}}|^2 \sum_{e=1}^6 \langle \chi_2|\chi_e\rangle\langle \chi_e|\chi_1\rangle.\end{aligned}\quad (28)$$

The summation is carried out over all nuclear spin sub-

levels of the excited state. With the help of Eq. (27) we factorize this sum into the magnetic-dipole matrix element μ_{12} , into the electric dipole matrix element μ_{opt} and into the overlap integrals of the nuclear spin-wave functions. The matrix elements μ_{12} and μ_{opt} are the same for all six configurations. If one assumes, that the sublevel population difference $\rho_{22} - \rho_{11}$ is the same for all subsets of atoms, $\rho_{22} - \rho_{11} \approx \Delta\rho$, the sum contains two overlap integrals between different nuclear spin states in the ground state but the same state $|\chi_e\rangle$ in the excited state.

The states $|\chi_e\rangle$ are eigenfunctions of the nuclear quadrupole Hamiltonian in the excited state and represent a complete set of basis states. The summation over all states

$$\sum_e |\chi_e\rangle\langle \chi_e| = \mathbb{1} \quad (29)$$

yields the unit operator and the expression for the signal reduces to

$$S \propto \mu_{12}|\mu_{\text{opt}}|^2 \Delta\rho \langle \chi_2|\chi_1\rangle = 0. \quad (30)$$

This result implies that all resonance lines in the ground-state spectrum, i.e., the central lines of the satellite spectrum, should vanish, provided that the sublevel population differences for all subsets of atoms are identical. This new interference effect originates from the large inhomogeneous line broadening and from optical transitions to all basis states of a complete set of eigenfunctions, which simultaneously contribute to the total signal. The interference can only be complete if the relevant sublevel population differences are identical for all signal contributions. An experiment with independent pump and test laser beams makes it possible to investigate the individual signal contributions separately to check how complete the predicted destructive interference is.

EXPERIMENTS

A. Experimental setup

The Raman heterodyne experiment with two independent laser beams is a combination of spectral hole burning¹⁹ and the conventional Raman heterodyne detection of NMR in impurity-ion solids.¹ To separate the various resonance lines, an accurate control of the frequency difference between pump and test laser beam is required. Figure 6 shows schematically the experimental setup. Both laser beams were derived from the same laser source (Spectra Physics 380 D), whose frequency jitter was some 500 kHz. The frequency of each laser beam was shifted with the help of an acousto-optic modulator (AOM). AOM1 and AOM2 were driven by two independent rf synthesizers with frequencies ω_1 and ω_2 , which allowed an accurate control of the frequency difference between pump and test laser beam. A weak resonant rf field (< 1 G) was applied along the crystal c axis and was used to drive the rf transition between two nuclear spin states.

The experiments were performed on the ${}^3H_4 \leftrightarrow {}^1D_2$ transition (610.7 nm) of Pr^{3+} ions in YAlO_3 (YAP) at low temperatures. Pump and test laser beams, which had a power of 10 mW and 14 μW , respectively, propagated

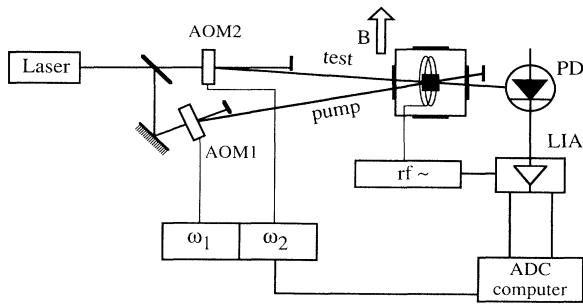


FIG. 6. Experimental setup: AOM—acousto-optic modulator, PD—photo diode, LIA—lock-in amplifier, rf~rf sweep generator, ω_1 and ω_2 high-frequency synthesizers.

along the crystal c axis at an angle of intersection of 5 mrad. The beat signal of the test laser field and the scattered Raman field was detected phase sensitively with a photodiode and a lock-in amplifier (LIA). To monitor the spectrum of the RHS the frequency of the test laser beam was varied relative to that of the pump laser beam with the help of AOM2 and the in-phase and out-of-phase parts of the RHS were detected simultaneously.

B. Radio-frequency spectrum

To avoid destructive interference effects from different Zeeman sublevels or nonequivalent lattice sites in Pr:YAP,⁷ an external magnetic field of 26 G was applied parallel to the principal Z axis of the quadrupole tensor of lattice site 1.

Figure 7 shows the absorptive part of the heterodyne beat signal for the transitions between the $|\pm\frac{1}{2}\rangle$ and $|\pm\frac{3}{2}\rangle$ nuclear spin sublevels in the electronic ground state of Pr:YAP. The two lines near 7.05 ± 0.08 MHz result from transitions of lattice site 2 [full width at half maximum (FWHM) 61 kHz] and the two lines near 7.05 ± 0.28 MHz result from transitions of site 1 (FWHM 47 kHz). This spectrum was recorded with two laser

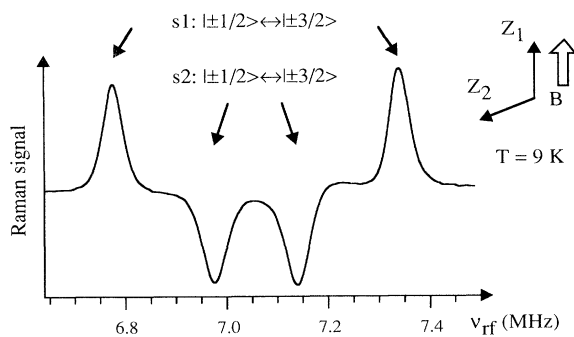


FIG. 7. Raman heterodyne beat spectrum in absorption for the 3H_4 $|\pm\frac{1}{2}\rangle \leftrightarrow |\pm\frac{3}{2}\rangle$ transitions of Pr³⁺YAlO₃. For the Raman heterodyne experiment with two laser beams, the radio frequency was set to the center of the resonance line near 6.97 MHz.

beams with identical frequencies ($\nu_T = \nu_P$), which corresponds to the conventional Raman heterodyne experiment. The spectrum shows that under these conditions all nuclear spin transitions of both nonequivalent lattice sites are well separated. In all experiments described in this article, the rf field was applied parallel to the principal X axis of the quadrupole tensor. The triple product of the transition matrix elements is then purely imaginary.

C. Laser frequency dependence

For the two-beam Raman heterodyne experiment, we chose a transition between two nuclear spin states in the electronic ground state of lattice site 2. The rf field ($\nu_{rf} = 6.97$ MHz) was resonant ($\delta_{rf} = 0$) with the transition between the $m_I = \frac{1}{2}$ and $\frac{3}{2}$ nuclear spin states in the electronic ground state of lattice site 2. Figure 8 shows both phases of the heterodyne beat signal as a function of the frequency difference between test and pump laser field. The dashed vertical lines indicate the positions of the ground state resonance lines, which can be calculated from the sublevel splittings in the electronic ground state of Pr:YAP. The spectrum of the RHS consists of five satellite spectra, which are centered at the positions of the ground-state resonance lines. Only one satellite spectrum can be observed for a positive laser frequency difference ($\nu_T - \nu_P > 0$). The line positions agree with the theoretical stick spectrum of Fig. 4, which was derived for the case of a negative quadrupole coupling constant in the electronic ground state. One can therefore conclude that the effective quadrupole coupling constant in the electronic ground state of Pr:YAP must be negative.¹⁸ To simplify the discussion of the spectrum of the RHS we approximate the ground-state sublevel splittings for site 2 by 7, 14, and 21 MHz and assume only three nondegenerate sublevels in the excited state.

The arrows in Fig. 8 indicate the position of a satellite line, where the dependence of the heterodyne beat signal on the radio frequency was measured for a fixed laser fre-

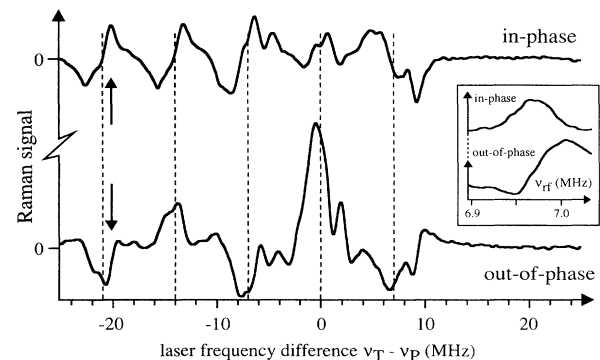


FIG. 8. Raman heterodyne signal of the $\frac{1}{2} \leftrightarrow \frac{3}{2}$ transition of site 2 for resonant excitation of the nuclear spin transition as a function of the frequency difference between test and pump laser beam. The dashed lines indicate the expected line positions in the ground-state spectrum. The inset shows the radio-frequency spectrum for the laser frequency difference indicated by the arrows.

quency difference. The inset of Fig. 8 shows the observed signal. With the name convention of the theoretical part of this article we call the absorptive signal component the in-phase part of the signal and the dispersive signal component the out-of-phase part of the signal. At the positions of the dashed lines, where the laser frequency difference exactly corresponds to a sublevel splitting in the electronic ground state, the absorptive in-phase part of the RHS always has a small signal amplitude.

With the knowledge of the energetic order of the nuclear spin states in the electronic ground state one can derive for each ground-state resonance line those optical transitions to which pump and test laser field couple at the given position in the spectrum. These different configurations were summarized in Fig. 4. In particular, one can derive from Fig. 4 that the satellite spectra near $\nu_T - \nu_P = -21$ MHz and $\nu_T - \nu_P = -14$ MHz are caused by anti-Stokes and Stokes Raman scattering of the test laser beam from the same sublevel coherence. For both spectra the same three subsets of atoms contribute to the satellite lines. For each subset the pump laser field drives one of the three possible optical transitions $|\Psi_g|\pm\frac{3}{2}\rangle \leftrightarrow |\Psi_e\rangle|\chi_e\rangle$. For both satellite spectra, the relevant sublevel population differences are equal and the same optical transitions determine the signal amplitudes of the satellite lines. Therefore the signal amplitudes of corresponding satellite lines should be identical in both satellite spectra. We use these two satellite spectra to compare the RHS for Stokes and anti-Stokes scattering with the predictions of Eq. (26).

For this comparison Fig. 9 shows the two satellite spectra on an extended frequency scale. The upper spectrum shows the in-phase part of the signal and the lower spectrum the out-of-phase component. The dashed vertical lines indicate the positions of the ground-state resonance lines where pump and test laser field couple to the same sublevels in the excited state. In the center of each satellite spectrum the in-phase part of the signal vanishes. Only two resonance lines are clearly resolved in each satellite spectrum. The separations of these two satellite lines from the dashed line correspond to sublevel splittings in the excited state. Each of these positions corresponds to the RHS of a single scattering path and should

therefore show the frequency dependence predicted by Eq. (23). In the experimental spectra, the resonance lines are broadened by the laser frequency jitter, but the resulting resolution allows still the verification that the in-phase part of the signal shows an absorptive dependence on the detuning of the test laser field, in agreement with Eq. (26).

A calculation of the signal amplitudes helped to confirm this interpretation of the satellite spectra. The amplitudes of the satellite lines are determined by the relevant sublevel population difference and by the matrix elements of the optical transitions to which the test laser field and the scattered Raman field couple at the given position in the spectrum. The calculated signal amplitudes are shown in Fig. 9 as individual resonance lines.

For each subset of atoms the sublevel population difference that results from the spectral hole burning by the pump laser field was calculated by numerical integration of coupled rate equations for the populations of the nuclear spin states.²⁰ Parameters for this calculation were the relative strengths of the optical transitions, the nuclear spin relaxation rates at a given temperature,²¹ and the excited-state lifetime.²² The relative transition strengths were calculated from the overlap integral (27) between corresponding nuclear spin eigenfunctions in the ground and excited states. To confirm the calculation, we compared the calculated sublevel populations with the experimental hole-burning spectrum and found good agreement. The upper inset of Fig. 9 summarizes the calculated sublevel population differences between the $|\pm\frac{1}{2}\rangle$ and $|\pm\frac{3}{2}\rangle$ ground-state sublevels for those atoms that contribute to both satellite spectra as a function of the laser frequency difference. A large population difference results only for atoms, for which the pump laser field couples to the $|g\rangle|\pm\frac{5}{2}\rangle \leftrightarrow |\pm\frac{3}{2}\rangle$ transition.

From the energy level scheme in Fig. 5, one can derive that these atoms give rise to satellite lines at exactly those positions, where the in-phase part of the observed signal has the largest amplitude, e.g., at $\nu_T - \nu_P = -(21 - 1.56)$ MHz and at $\nu_T - \nu_P = -(21 + 0.92)$ MHz. However, the same atoms also contribute to the ground-state resonance line in the center of each satellite spectrum, where the ob-

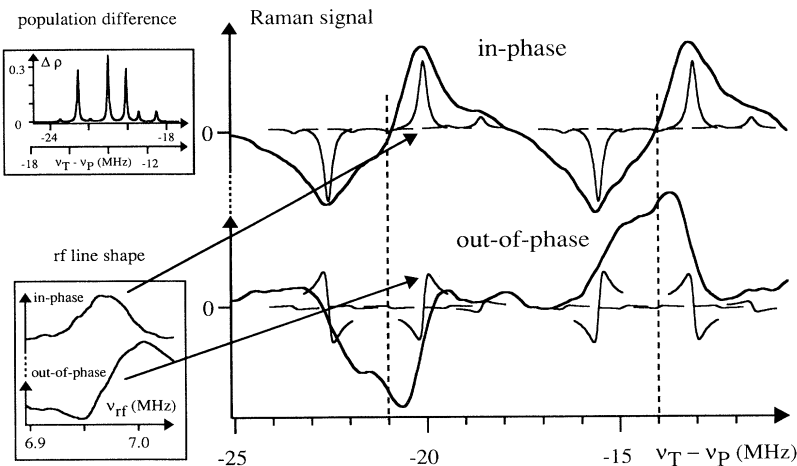


FIG. 9. In-phase (top) and out-of-phase (bottom) part of the two-beam RHS on an extended frequency scale. The upper inset shows the calculated population difference between the $|\pm\frac{1}{2}\rangle$ and $|\pm\frac{3}{2}\rangle$ nuclear spin states in the electronic ground state. The lower inset shows the observed dependence on the rf detuning for the satellite line at $\nu_T - \nu_P = -(21 - 0.92)$ MHz.

served signal vanishes. To calculate the actual amplitude of the RHS, we multiplied for each resonance line the sublevel population difference by the triple product of the relevant transition matrix elements. The absorptive and dispersive lines in Fig. 9 represent the calculated signal amplitude. A large signal amplitude results only for two satellite lines, but not for the central ground-state resonance line, where the transition matrix elements are small.

The signal amplitudes in both satellite spectra are identical, because for corresponding satellite lines the same optical transition matrix elements determine the signal amplitude. The in-phase part of the RHS shows an absorptive dependence on the detuning of the test laser field for Stokes and for anti-Stokes scattering. The dispersive out-of-phase part, however, changes its sign for Stokes vs anti-Stokes scattering. The observed dependence on the detuning of the rf field and test laser field is in agreement with the behavior predicted by Eq. (26). In the derivation of the heterodyne signal, we did not discuss the mechanism of the line broadening of the optical transitions. The observed width of the satellite lines, however, indicates that the linewidth in this experiment was determined by the width of the spectral holes, which was of the order of 1 MHz due to the laser frequency jitter. The base line of the experimental signal seems to be distorted for all satellite spectra. This might be due to absorption of the test laser field or the scattered Raman field in the crystal, which was neglected for the theoretical description of the coherent Raman scattering.

D. Interference effects

With this assignment of the in-phase and out-of-phase part of the RHS we will now discuss the interference of scattering paths. Figure 10 shows the absorptive in-phase part of the RHS for the satellite spectrum near $\nu_T - \nu_P = +7$ MHz on an extended frequency scale. The dashed horizontal line represents the signal base line and the dashed vertical line in the middle of the spectrum indicates the position of the expected ground-state resonance line. From the energy level scheme of Fig. 4 one can derive that three subsets of atoms contribute to the

signal at this position. For all three subsets, the pump laser field couples the $|\Psi_g\rangle|1/2\rangle$ state to one of the $|\Psi_e\rangle|\chi_e\rangle$ states, while the test laser field couples the $|\Psi_g\rangle|3/2\rangle$ state to the same excited state. Under the experimental conditions the optical pump rate of the pump laser field was large in comparison to the spontaneous decay rate of the excited state. Therefore the pump laser field depletes the resonant ground-state sublevel $|\Psi_g\rangle|1/2\rangle$ almost completely for all three subsets of atoms. The calculated sublevel population differences for this satellite spectrum are shown in the inset of Fig. 10. For each of the three subsets of atoms the population difference between the $m_I = 1/2$ and $3/2$ sublevels in the electronic ground state is almost identical. This is exactly the condition which has to be satisfied for interference between scattering paths, which can be predicted for the ground-state line in the center of this satellite spectrum.

The narrow absorption lines in Fig. 10 represent the calculated signal amplitudes for all satellite lines. Four of the satellite lines, corresponding to the test laser-field coupling to the $|\Psi_g\rangle|3/2\rangle \leftrightarrow |\Psi_e\rangle|\pm 5/2\rangle$ or $|\Psi_g\rangle|3/2\rangle \leftrightarrow |\Psi_e\rangle|\pm 1/2\rangle$ transition, have large signal amplitudes, indicating that the optical transition matrix elements are large. For the third optical transition, $|\Psi_g\rangle|3/2\rangle \leftrightarrow |\Psi_e\rangle|\pm 3/2\rangle$, the relevant transition matrix elements are smaller. The same atoms that contribute to the satellite lines simultaneously contribute to the central ground-state line, at the position of the dashed vertical line near $\nu_T - \nu_P = +7$ MHz. However, the two main signal contributions to the ground-state line have opposite amplitudes. The individual signal contributions interfere destructively, which results in the small signal amplitude of the central ground-state line. It is obvious that the largest signal amplitude was not observed for the central ground-state line but for neighboring satellite lines, e.g., near $\nu_T - \nu_P = -9.5$ MHz, although only one subset of atoms contributes to the satellite lines but three subsets to the central ground state line.

The cancellation of the different signal contributions to the ground-state line is a direct consequence of the fact that the nuclear spin sublevels of the excited state represent a complete set of functions. If the sublevel pop-

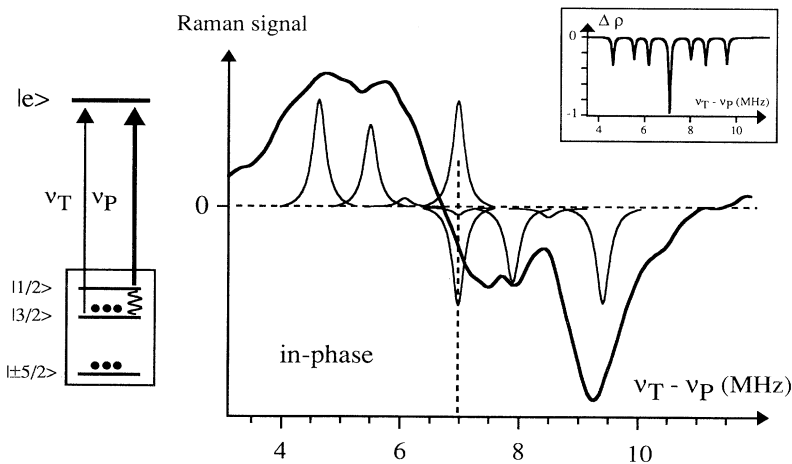


FIG. 10. Interference of scattering paths in the center of the satellite spectrum. At this position the test laser field can simultaneously couple to all optical transitions between one ground-state and all excited-state sublevels for different subsets of atoms. The inset shows the calculated sublevel population differences, which are nearly identical for all subsets of atoms.

ulation differences of all three subsets of atoms were equal, this would result in a vanishing signal amplitude for the central ground-state resonance line. The satellite spectrum in Fig. 10 is a clear proof that the predicted destructive interference exists. The interference is not complete, however, because of small variations of the spectral hole burning for different subsets of atoms. The same destructive interference effect was also observed for the corresponding anti-Stokes scattering at $\nu_T - \nu_P = -7$ MHz (compare with Fig. 8).

E. Discussion

The interference of scattering paths that we have demonstrated here occurs also in the conventional Raman heterodyne experiment with a single laser beam.¹ The single-beam experiment corresponds to a two-beam experiment with equal pump and test laser frequencies, whose signal amplitude can be observed at the origin of the frequency axis in Fig. 8. The signal at this position includes Stokes and anti-Stokes contributions. To get an idea of the individual contributions, we note that the same atoms also contribute to the ground-state resonance lines at $\nu_T - \nu_P = \pm 7$ MHz. The signal at +7 MHz, e.g., represents Stokes scattering from the same atoms that contribute to the zero-frequency line by anti-Stokes scattering. Since the in-phase part of the signal at $\nu_T - \nu_P = \pm 7$ MHz has comparable amplitudes but opposite signs, we expect destructive interference of the two remaining signal contributions at $\nu_T = \nu_P$.

The out-of-phase part of the signal shows a large signal amplitude close to zero frequency. They cannot arise from the true ground-state resonance line, whose signal would cross through zero at this point. An analysis of the different contributions shows that it is due to the superposition of two dispersive signal contributions of neighboring satellite lines. This signal is significantly larger than the absorptive in-phase part and is the main signal in the conventional Raman heterodyne experiment with a single laser beam. Since the observed signal arises primarily from satellite lines, we conclude that some laser frequency jitter is actually useful in the conventional experiment. The maximum of the signal is slightly displaced from zero and only the relatively large linewidth, which arises from the frequency jitter, provides for a nonvanishing amplitude at zero frequency. In systems with larger sublevel splittings in the excited state, the absolute maximum of the signal amplitude should occur for larger laser detunings. We could verify this prediction experimentally in the related system $\text{Pr}^{3+}\text{Y}_2\text{SiO}_5$.

CONCLUSION

In this article we have described an interference effect that occurs in Raman heterodyne detection of nuclear spin transitions. In contrast to the Zeeman or site interference effects that have been reported earlier, it arises from a single magnetic dipole transition in one atomic species when different pathways contribute to the Raman scattering process. This is always the case in inhomogeneously broadened systems with a nonvanishing nuclear spin, and the effect persists in magnetic fields. A destructive interference results if these scattering paths include a complete set of functions, e.g., as in the case of our experiments all eigenfunctions of the nuclear quadrupole interaction in the excited state. The destructive interference can be complete if the relevant sublevel population differences are identical for all subsets of atoms that contribute to the total signal. We developed a pump-and-probe technique to study and circumvent the effect. An experiment on the rare-earth ionic solid $\text{Pr}^{3+}:\text{YAlO}_3$ clearly showed the predicted interference effect, although the destructive interference was not complete, as one can expect for different population differences in different subsets of atoms. In the conventional Raman heterodyne experiment, where the same laser beam acts as pump and test laser beam, the destructive interference between the different scattering paths leads to a reduced signal and can result in complete signal cancellation.

In this article we have discussed the dependence of the heterodyne beat signal on the detuning of the rf field and the test laser field. While the interpretation of the two-beam Raman heterodyne spectrum for this system was facilitated by the advantageous difference of the sublevel splittings in the ground and the excited state, similar experiments are also possible for related systems where this is not the case. For the interpretation of these spectra, the knowledge of the sublevel splittings in the ground and excited states is helpful. Conversely, the pump-and-probe technique allows to measure these splittings, including the energetic sequence of the nuclear spin states.

ACKNOWLEDGMENTS

We gratefully acknowledge the generous loan of the YAP crystal by Professor J. Mlynek and helpful discussions with Professor R. Kind. This work was supported by the Schweizerischer Nationalfonds.

¹N. C. Wong, E. S. Kintzer, J. Mlynek, R. G. DeVoe, and R. G. Brewer, *Phys. Rev. B* **28**, 4993 (1983).

²L. L. Wald, E. L. Hahn, and M. Lukac, *J. Opt. Soc. Am. B* **9**, 784 (1992).

³J. Mlynek, N. C. Wong, R. G. DeVoe, E. S. Kintzer, and R. G. Brewer, *Phys. Rev. Lett.* **50**, 993 (1983).

⁴Y. Takahashi, K. Ishikawa, T. Tanaka, Y. Fukuda, H. Hatana, and T. Hashi, *Phys. Rev. B* **38**, 7121 (1988).

⁵Y. Takahashi, K. Ishikawa, Y. Fukuda, T. Yabuzaki, and T.

Hashi, *Phys. Rev. B* **43**, 7527 (1991).

⁶M. Mitsunaga, E. S. Kintzer, and R. G. Brewer, *Phys. Rev. Lett.* **52**, 1484 (1984).

⁷M. Mitsunaga, E. S. Kintzer, and R. G. Brewer, *Phys. Rev. B* **31**, 6947 (1985).

⁸L. E. Erickson, *Phys. Rev. B* **42**, 3789 (1990).

⁹L. E. Erickson, *J. Phys. C* **20**, 291 (1987).

¹⁰N. B. Manson, P. T. H. Fisk, and X.-F. He, *Appl. Magn. Reson.* **3**, 999 (1992).

- ¹¹J. A. Giordmaine and W. Kaiser, *Phys. Rev.* **144**, 676 (1966).
- ¹²R. G. Brewer and E. L. Hahn, *Phys. Rev. A* **8**, 464 (1973).
- ¹³P. D. Bloch, W. Brocklesby, R. Harley, and D. R. Taylor, *J. Phys. (Paris) Colloq.* **46**, C7-523 (1985).
- ¹⁴E. S. Kintzer, M. Mitsunaga, and R. G. Brewer, *Phys. Rev. B* **31**, 6958 (1985).
- ¹⁵M. H. Cohen and F. Reif, *Solid State Phys.* **5**, 321 (1957).
- ¹⁶A. Abragam and B. Bleaney, *EPR of Transition Ions* (Clarendon, Oxford, 1970).
- ¹⁷M. A. Teplov, *Sov. Phys. JETP* **26**, 872 (1968).
- ¹⁸T. Blasberg and D. Suter, *Phys. Rev. B* **48**, 9524 (1993).
- ¹⁹S. Völker, *Annual Review of Physical Chemistry*, edited by H. L. Strauss, G. T. Babcock, and C. B. Moore (Annual Reviews Inc., Palo Alto, CA, 1989), Vol. 40, p. 499.
- ²⁰J. P. D. Martin, N. E. Rigby, and N. B. Manson, *J. Lumin.* **55**, 31 (1993).
- ²¹T. Blasberg and D. Suter, *Chem. Phys. Lett.* **215**, 668 (1993).
- ²²R. M. MacFarlane and R. M. Shelby, in *Spectroscopy of Solids Containing Rare Earth Ions*, edited by A. Kaplyanskii and R. M. MacFarlane (North-Holland, Amsterdam, 1987).